DTU Library

Operational Modal Analysis and Fluid-Structure Interaction

Vigsø, M.; Kabel, T.; Tarpø, M.; Brincker, Rune; Georgakis, C.

Link back to DTU Orbit

Operational Modal Analysis and Fluid-Structure Interaction

M. Vigsø [1]**, T. Kabel** [1]**, M. Tarpø** [1]**, R. Brincker**[2] **and C. Georgakis** [1]
[1] Aarhus University, Department of Engineering,
Inge Lehmanns Gade 10, 8000 Aarhus, Denmark
e-mail: **mvigso@eng.au.dk**

[2] Technical University of Denmark, Department of Civil Engineering,
Brovej Building 118, 2800 Kgs. Lyngby, Denmark

Abstract

Operational modal analysis (OMA) has in the last decade shown its potential in the field of offshore structures such as oilrigs and wind turbines etc. Typically, the estimated modal parameters will be used in conjunction with a finite element (FE) model. However since bottom-fixed offshore structures typically will be semi-submerged this affects the modal parameters by fluid-structure interaction. Fluid surrounding a structure is known to retard the response and locally introduce an increase in mass and damping. These local changes yield a complex alteration of the modal parameters and this paper highlights these effects by a wave flume experiment conducted on a cantilever structure. The structure is a scaled offshore structure and its modal parameters are examined at different water levels ranging from dry state to 60 % submerged.

1   Introduction

Modal analysis is an effective tool in describing the dynamic behaviour of a structure. When dealing with civil engineering structures, traditional experimental modal analysis (EMA) has some shortcomings and hence opens the playground for its cousin named operational modal analysis (OMA). OMA utilizes the operational conditions in providing the excitation of the structure and if the loading is approximating white noise, the modal parameters can elegantly be extracted from the structural response. The application of OMA is gaining ground and is becoming the preferred approach when evaluating modal properties of offshore structures [16]. The motivation for making modal analysis may be multiple; for instance in the field of structural health monitoring (SHM), model updating, fatigue estimation or indirect load estimation. Most of these disciplines use an FE model (updated to insitu conditions) as a basis.

There will always be some natural variations in the estimated modal parameters; besides estimation- or statistical error also environmental changes such as wind speed, scour or other seabed changes, structural degradation, mass loading, temperature or even tidal variations can cause the modal parameters to fluctuate. This paper will focus on how variations in the surrounding water may alter the dynamics of the structure.

The fluid-structure interaction is a complex topic and existing research in this area is plentiful. Both analytical, experimental and numerical work has been done in the past, e.g. [8, 12, 15, 18]. The content of this paper does not intend to challenge these works, instead it will demonstrate an application in the field of operational modal analysis conducted on a miniature offshore model. The results shown in this paper are preliminary findings which will be the basis for a later study, where an accurate model update is required. The model design does not descend from any actual physical structure, but is constructed as a simple cantilever with a topside in order to better monitor the torsional modes.

2 Experiment setup

The experimental campaign is conducted at Luminy University at Marseille, France in 2018. A cantilever structure made from plexiglass will be the scope for this study. The structure is a cylindrical mono tower with a truss box topside. The columnar part of the model is constructed by segments bolted together through an internal flange. Each segment is 200 mm in length and has an outer diameter of 150 mm. The structure is dry on the inside at all times during the tests. The topside has an outer geometry of $l \times b \times h$ of $400 \times 200 \times 200$ mm. The entire model is situated on a load cell connected to an aluminium base plate, which yields a total height of the model to be 1485 mm. The maximum water level, which can be applied in the flume, is 900 mm as indicated by Figure 1 a) and b). The sizing of the segments is primarily based on accessibility concerns regarding sensor installation. The joints between the circular sections are waterproofed through a gasket which may be seen in Figure 1 c).

The model is equipped with 16 uni-axial accelerometers; nine of which are positioned inside the pile and the remaining seven are distributed to the corners of the topside. The position and measuring direction are indicated in Figure 1 b). The accelerometers used are Brüel & Kjær TYPE 4508-002 1000 mV/g and the sampling rate is 2 kHz.

The scope of the test is to monitor the structure during water filling of the flume and track the changes in modal parameters due to the influence of water. The test will begin at zero water level (referred to as dry state) and the water level will be increased to a maximum of 900 mm. Intermediate tests are conducted at 150 mm, 400 mm, 670 mm, 800 mm and 850 mm respectively. For each of these water levels, 3-4 individual tests are performed. The tests are conducted by introducing some random loading to the structure and record the response for approximately 300 seconds. The concepts of operational modal analysis are then applied on the response data from the accelerometers and modal parameters (natural frequencies, damping ratios and mode shapes) are extracted [6].
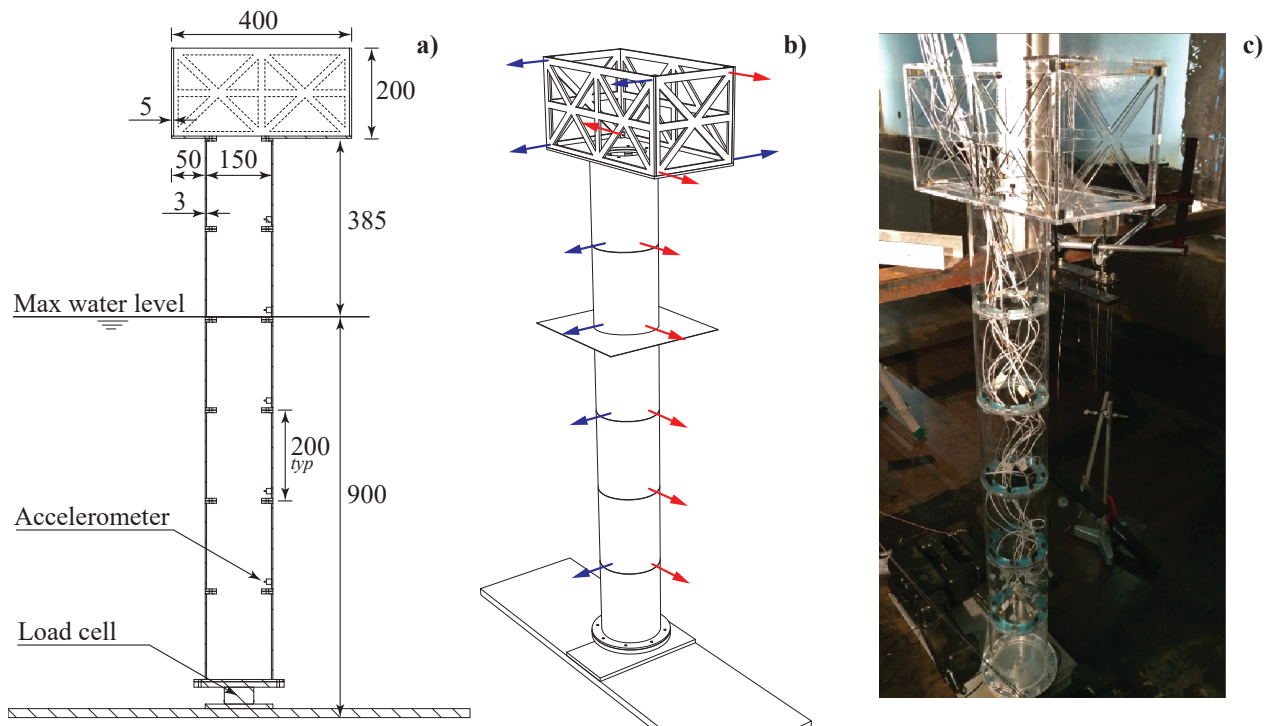

Figure 1: Experimental setup. a) shows the sideview cross section including the overall dimensions of the model, b) indicates the sensor position and direction, c) shows a picture from the test. Dimensions in mm.

In order for OMA to be successfully applied, the loading of the structure should be approximately white noise i.e. random in time and space [6]. The excitation medium utilized in this case is a soft brush swept over the structure along with disturbance to the surrounding water.

Additional instrumentation not relevant for the topic of this paper includes: ATI 6 DOF load cell, Wave gauges, 8 pcs kulite pressure transducers. These are installed for a later purpose in the test campaign.

3   ID algorithm

A total of 22 tests are conducted and though of different quality, each of these will yield an estimate on a number of modes. The frequency band of interest is 0 - 160 Hz as anything above this is too inflicted by noise and the sensor resolution not capable of spanning the modes shapes. Nine modes are identified in this frequency band and these nine modes will be examined in greater detail.

Now, several different identification methods are available both in the time domain and in the frequency domain. The identification algorithm selected is the Time Domain Poly Reference (TDPR) [17]. Although it was developed for impulse response functions, it can easily be adopted in OMA by using the correlation functions instead [5, 11]. Note that this section is not intended to go into details on the algorithm, however a brief overview of the method is outlined. For further details, the reader may find use of literature such as [6, 9].

Basically the response data of the structure are used to calculate the correlation functions. The transposed correlation function matrix is then considered as free decays of the system and the concepts of the TDPR can be applied; A Hankel matrix is constructed and the polynomial coefficients are solved by a least square approach. Then, the coefficients are stored in a companion matrix and by making an eigenvalue decomposition, the modal parameters can be found.

Now, in order to get the best conditions for the modal identification, filtering and DOF condensation are applied as a pre-step to the TDPR. This is exercised in the frequency domain by reducing the number of DOFs and amplifying the remaining principal components. The details on condensation can be found in [13].

The data is examined by looking at one frequency band at a time. While moving the frequency band and shifting the model order in the TDPR, stable poles are extracted from the signal. Typically these are represented by stabilization diagrams, but in order to limit the data flow in the figures of this paper, only the single picked modes are shown.

4   Modal parameter tracking

To give an indication of the quality of the data, a compilation of spectres are shown in Figure 2. The data series for each water level are merged into a single file and the spectra are averaged using the Welsh technique with a block size of 2^{13} samples corresponding to four seconds. A singular value decomposition of the spectral density is made and the figure shows the first three singular lines. The modes in Figure 2 are identified by peak picking and tracked by colour coding.
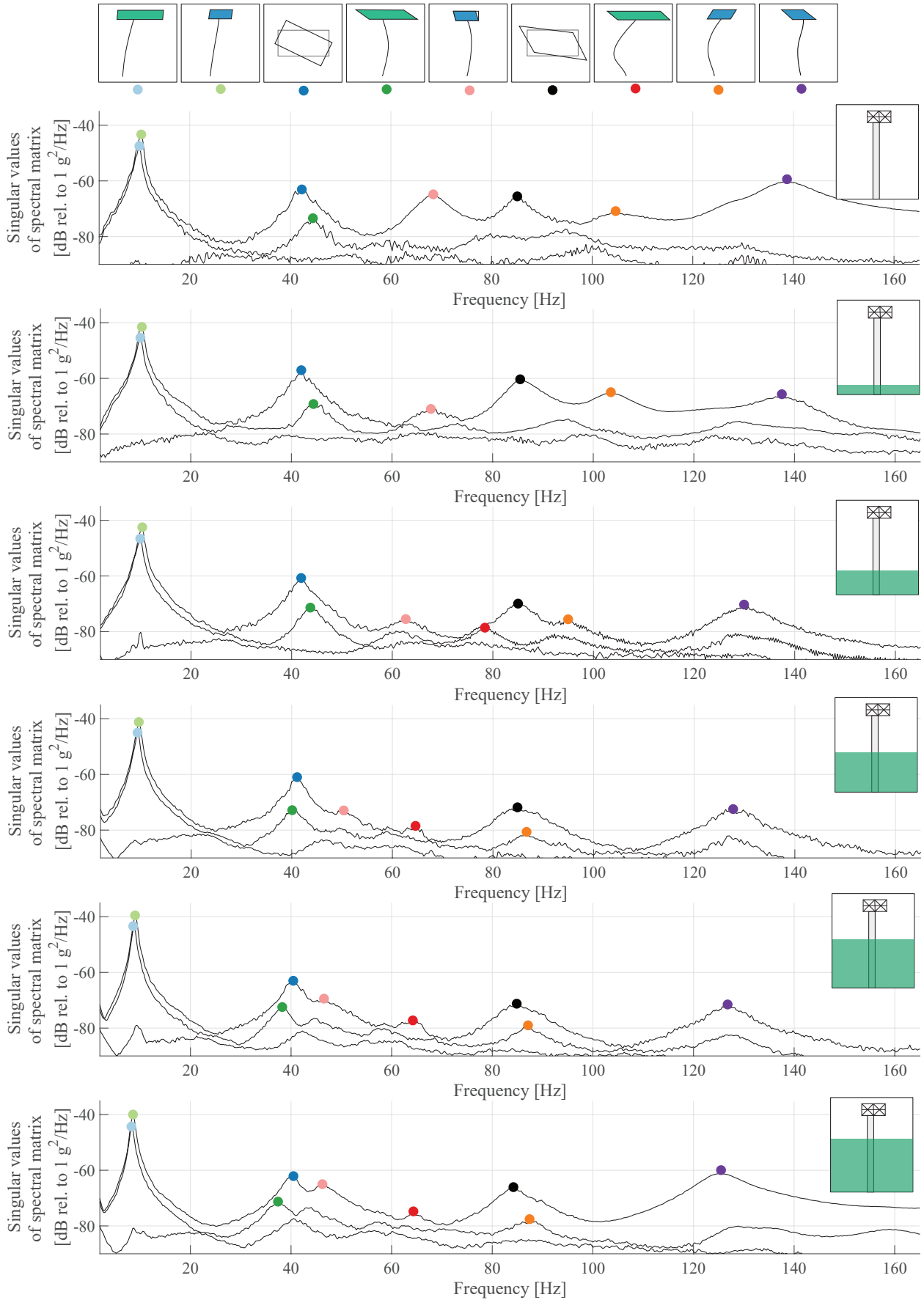
Figure 2: Singular values of the spectral density. The 3 first singular values are shown for different water levels. The water levels shown are 0, 150, 400, 670, 800 and 900 mm respectively. The different mode shapes identified are sketched in the top of the figure in ascending order and indicated by a coloured dot.

5 Results

For the seven different water levels ranging from 0 to 900 mm, modal identification is conducted using the TDPR technique outlined in Section 3. For each water level, 3-4 separate tests are made and the modal parameters are shown along with the average of the estimates. Figure 3 and Figure 4 show the identified modes in the frequency band of 0-160 Hz. The natural frequency, damping ratio and mode shape complexity are all given as a function of the water level. The individual mode shapes (1-9) are sketched in Figure 2 for reference.

The data in Figure 4 are merely the same as given in Figure 3, but normalized with respect to the average dry conditions to show the relative development in modal parameters.

As seen in Figure 3 and 4, the scatter in the estimates are significantly higher on the damping ratios and complexity indicators than for the frequencies. This is not uncommon when engaging in modal analysis on experimental data (especially when dealing with closely spaced modes), yet it masks the conclusion on the fluid influence on these parameters - more about this in the following.

First, looking at the frequencies; it is seen that in general the natural frequencies drop with the increase in water level due to the hydrodynamic added mass. Yet, mode 3 and mode 6 are nearly unaffected by the water. The mode shapes for these are characterized by predominant deformation to the topside and nearly no subsea deformation, see Figure 2. Literature such as [3, 4] states that one may encounter these effects when fluid-structure interaction is present. Since all modes, but the ones concerning only the topside, have a decrease in frequency, this yield an interesting phenomena as the modes start to cross each other by frequency. This is seen in Figure 3 a) at a water level of 670 mm for mode 3 and at a water level of 250 mm for mode 6.

Next looking at the damping estimates; the scatter from test to test is high compared to the average changes due to the influence of water. However, there is a tendency of an increase in damping for all modes. The higher modes (with exemption to mode 6) seems to be affected the most with respect to the damping with relative changes > 30 % whereas the the changes on the first two bending modes and the two topside modes are less significant, see Figure 4 b).
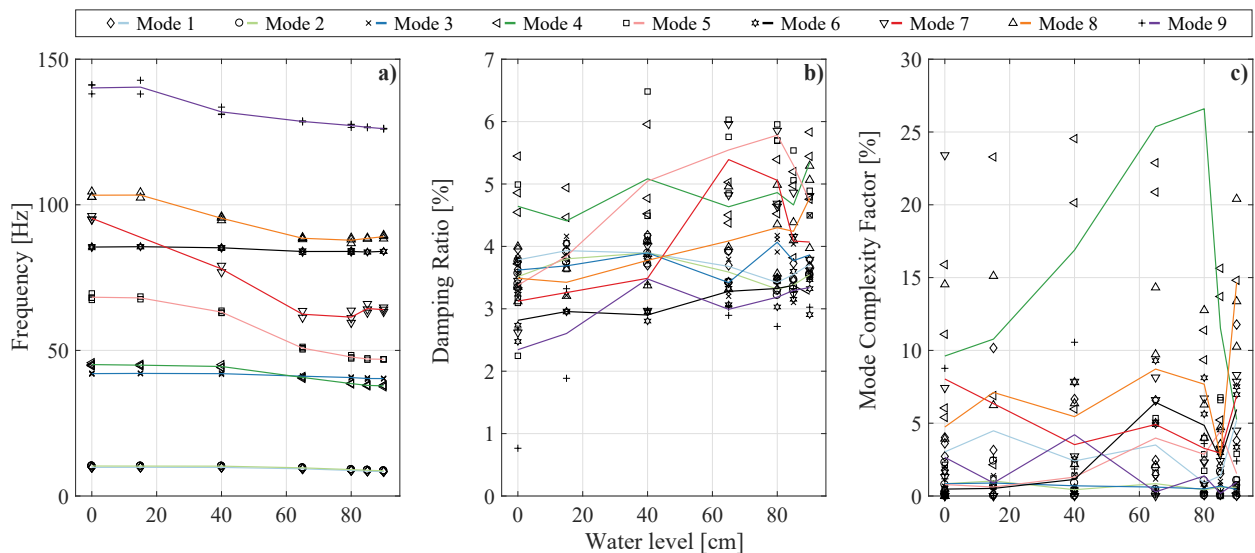

Figure 3: Estimated modal parameters at different water levels. Each mark represents an estimate from a data series and the solid lines are the water level averages. a) shows the development in natural frequency for each mode. b) shows the development in damping ratio for each mode. c) shows the development in mode shape complexity of each mode.
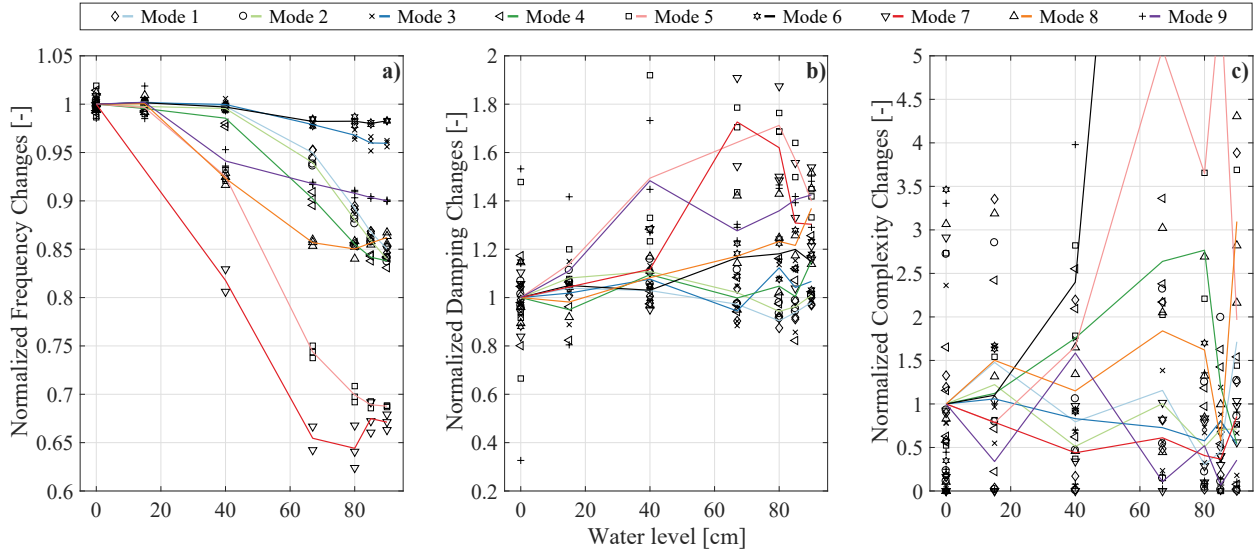
Figure 4: Relative changes in modal parameters due to shift in water level. Each mark represents an estimate from a data series and the solid lines are the water level averages and normalized with respect to the dry state. a) shows the relative development in natural frequency for each mode. b) shows the relative development in damping ratio for each mode. c) shows the relative development in mode shape complexity of each mode.

Finally, the complexity of the mode shapes are shown in Figure 3 c) and Figure 4 c). The details on how the mode complexity factor is calculated is described in Section 6.1. In general there is a considerable level of complexity in the mode shapes ranging between 1 and up to 30 %. However, given the level of scatter in the estimates it is inconcludable whether the complexity originates from the influence of water or rather non-linearities in the model. The latter is anticipated to be the main reason for the complexity considering the number of structural joints, material selection etc.

6 Mode shape alteration

6.1 Complex mode shapes

When identifying mode shapes from experimental data, often the identified mode shapes tend to have a imaginary part. This may be due to ID algorithm, non-linearities or cases of non proportional damping. The complex part is often considered as noise and disregarded, but it may indicate some physical properties of the system [10]. If the purpose of the modal analysis is to link the experimental mode shapes to ones obtained from an FE model, the most natural choice would be to disregard the imaginary part or use the absolute value.

Several different indicators can be used to quantify the complexity in a mode shape. For this case the mode complexity factor (MCF) will be utilized. The MCF is calculated for mode r as

$$\text{MCF}_r = 1 - \frac{(S_{xx} - S_{yy})^2 + 4S_{xy}^2}{(S_{xx} + S_{yy}^2)} \tag{1}$$

where

$$S_{xx} = \Re\{\psi_r\}^T \Re\{\psi_r\} \qquad S_{yy} = \Im\{\psi_r\}^T \Im\{\psi_r\} \qquad S_{xy} = \Re\{\psi_r\}^T \Im\{\psi_r\} \tag{2}$$

Here $\{\psi_r\}$ is the mode shape vector for mode r. The MCF value is real and ranging between 0 and 1.
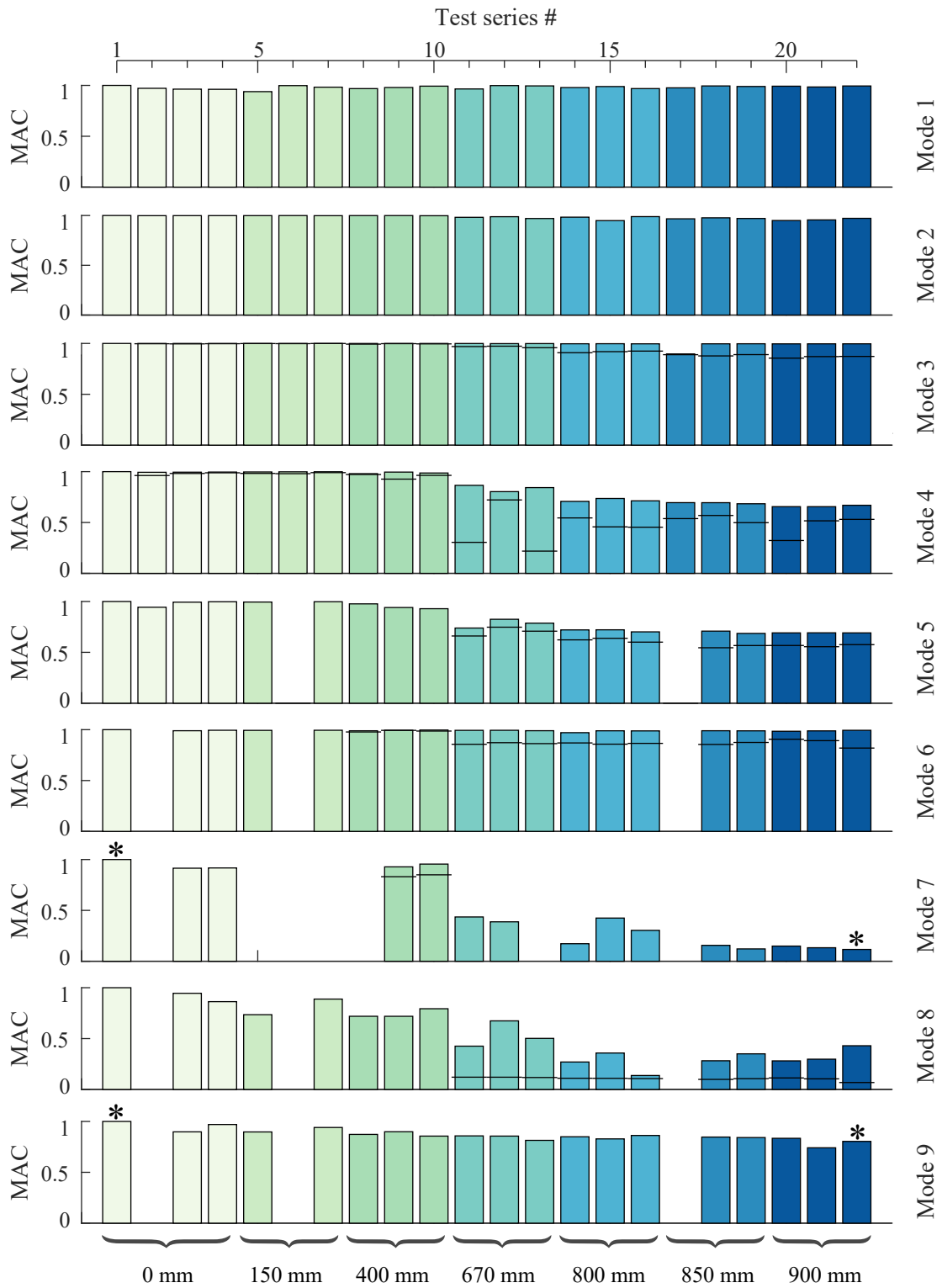
Figure 5: Modal assurance criterion (MAC). Every column corresponds to a test series while every row corresponds to a mode. The columns are grouped according to water level during the test. The black line splitting a single bar indicates the MAC value prior to rotating the mode shapes within their subspace. The four estimates marked by an asterisk (*) are shown in Figure 6 and Figure 7.

6.2 Mode shape

For complex modes, the MAC value between two mode shape vectors $\{\psi_a\}$ and $\{\psi_b\}$ can be calculated from [1, 14] as

$$\text{MAC}(\{\psi_a\}, \{\psi_b\}) = \frac{|\{\psi_a\}^T\{\psi_b\}^*|^2}{(\{\psi_a\}^T\{\psi_a\}^*)(\{\psi_b\}^T\{\psi_b\}^*)} \tag{3}$$

In order to quantify the changes in mode shapes the MAC value is calculated for every mode compared to a reference mode shape. The reference mode shape is the mode shape at dry state identified by the first test series - i.e. the first column in Figure 5. The MAC values depicted are hence the same mode for all successive tests compared to the reference test.

When modes are closely spaced in frequencies, their associated modes shapes may be rotated within the subspace spanned by the modes engaged [2]. For instance, this can be observed in the case of mode 3, 4 and 5 whose mode shapes start to mix at a water level of 670 mm, see Figure 3 a) or Figure 2. How much the mode shapes will blend among the conjointly modes depends on ID algorithm used and its fitting parameters. Surely it is more convenient if this rotation does not occur, but it does not pose a problem as they can be reorientated to fit the reference modes better. This is done by assuming a linear combination of the mode engaged and making a least square fit to the reference modes.

Test series 2, 6 and 17 showed poor results due to improper excitation. As a result of this, only the first 4 modes were extractable from the data, hence the missing bars in Figure 5. Although a true random excitation was attempted also mode 7 was not greatly engaged in several tests as seen from the spectra in Figure 2, this may be the reason for increased fluctuations in the estimates.

6.3 Mode shapes in details

In this section, a close-up on two selected mode shapes is presented. The mode shapes displayed are mode 7 and mode 9 which are highlighted by an asterisk (*) in Figure 5. The mode shapes have been normalized to a maximum deflection of 0.15 m i.e. 10 % of the total height of the model.

Note that the mode shapes presented by Figure 6 and 7 are shown by utilizing some assumptions on the behaviour of the structure. By looking at Figure 7 a), it is clear that the nodal value for the 4th node from bottom is incorrect. Since no sensor is positioned at this node in this direction the nodal value depicted is simply an interpolation value between the adjacent nodes. These assumptions are just for visualization purposes and do not influence the MAC values presented earlier. Same applies to the topside.
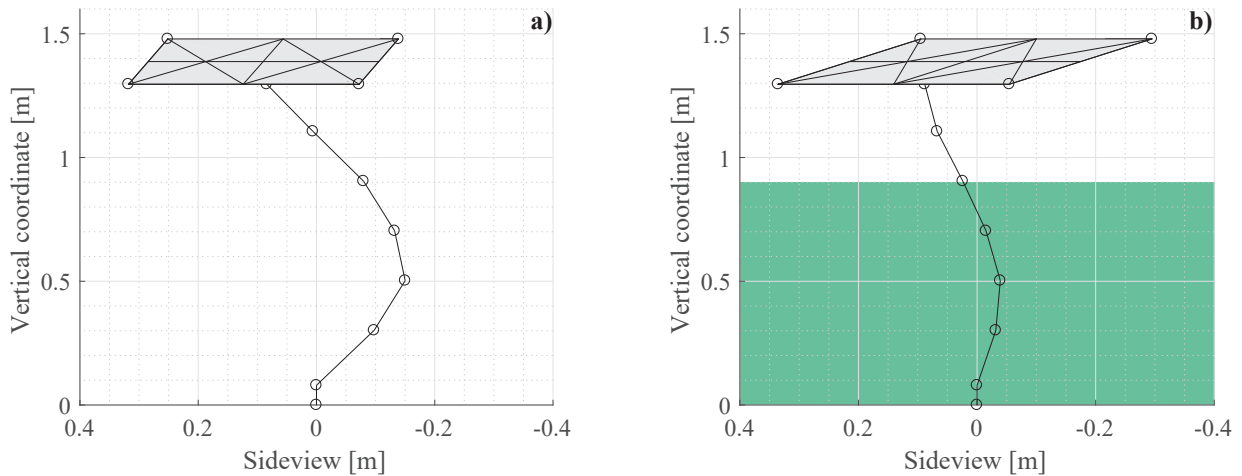

Figure 6: Mode shape 7 before and after water filling. MAC value between the two modes is 0.12.
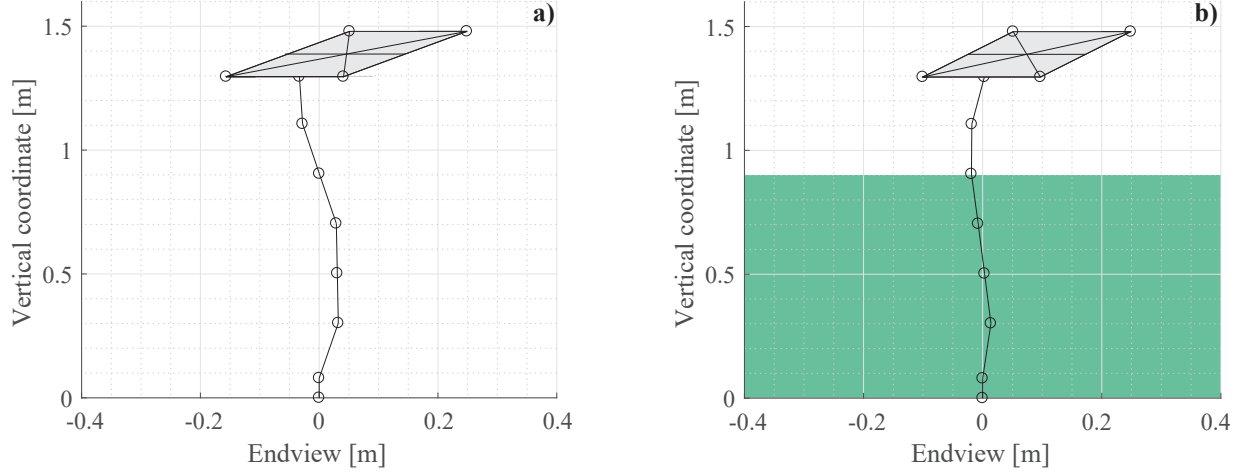
Figure 7: Mode shape 9 before and after water filling. MAC value between the two modes is 0.80.

Looking at these two modes shown by Figure 6 and Figure 7, the changes in mode shape are predominant subsea where the bending amplitude of the pile is reduced. The nodal point (zero vibration amplitude) for the pile is moved down for both cases.

7   Full scale perspective

The model considered in this paper is constituted as a hollow plexiglass model with a fairly large diameter to water depth ratio. This yields a large volume of water to be displaced by the structure and hence a large amount of added mass. Since the model itself is made from light weight material and air filled, the ratio of added mass versus the mass of the structure is also large. In the full scale perspective, the mass of the displaced water compared to the structural mass is likely to be a different ratio.

Now, if the structure is considered as an idealized SDOF system, the natural angular frequency is found as

$$\omega_{dry} = \sqrt{\frac{K_{dry}}{M_{dry}}} \tag{4}$$

where the K_{dry} is the generalized stiffness of the structure and M_{dry} is the generalized mass both at a dry state for a mode of vibration. If it is assumed that the stiffness of the structure is unchanged by the presence of water, the equation for the wet conditions becomes:

$$\omega_{wet} = \sqrt{\frac{K_{wet}}{M_{wet}}} = \sqrt{\frac{K_{dry}}{M_{dry} + M_{added}}} \tag{5}$$

Here, M_{added} symbolizes the added mass from the fluid- structure interaction [4, 12, 18]. Now, this is strictly only valid if the mode shape of interest is unchanged by the influence of water. This is a fair assumption for the first few modes in this case, see Figure 5. The change in frequency from the influence of water is hence seen as

$$\frac{\omega_{wet}}{\omega_{dry}} = \frac{1}{\sqrt{\left(1 + \frac{M_{added}}{M_{dry}}\right)}} \tag{6}$$

From equation (6) it is evident that the change in frequency depends on the ratio between the mass of the structure and the added mass from the fluid. Since the cross section of the model in this case is circular, there is no cross coupling and the added mass is somewhat proportional to the mass of the fluid displaced

by the structure: $M_{added} \propto V, \rho_w$, where V is the displaced volume and ρ_w is the fluid density. However other aspects such as boundary conditions for the fluid, viscosity, vibration amplitude and frequency can also influence the effect of added mass [4, 7]. Since the fluid density in this scaled experiment is larger than in full scale the effect from the fluid- structure interaction is amplified. This means that the relative changes in modal parameters shown by Figure 3 and Figure 4 may be less for the full scale scenario.

The model considered in this paper is dry on the inside (concerning the sensors). Offshore mono tower structures may be constructed as dry or wet on the inside where the latter is the most common. Water inside the structure will yield a different alteration of the structure as the internal water will further increase the added mass. This effect is not studied additionally but is worth mentioning.

8 Conclusion

This paper has outlined the changes in modal parameters from the influence of surrounding water on a small scale model. The model is a bottom fixed, surface piercing mono tower made from plexiglass. It was through operational modal analysis demonstrated how the modal parameters changes by the presence of water. Most significant finding was that the order of the modes were changing as the flume was filled with water. This was due to the nature of the individual mode shapes; mode shapes, where deflection is predominant ascribed to rotation and not bending of the tower will yield little or no changes from the water whereas especially higher order bending of the tower will experience great influence from the added mass. If modes are closely spaced this may cause them to change order.

Damping estimates were examined and found to increase with water level as expected. For semi-submerged structures, where fluid-structure interaction is present, it might be expected that non-proportional damping could cause the mode shapes to become complex. However it was not possible to show a decisive relation for this due to the scatter in the estimates. The mode shapes, however, were examined in details and it was seen that especially for higher modes; the deflection subsea were reduced.

The development in modal parameters are based on averages from different tests, where it was assumed that the water yields a constant alteration of the modal parameters. The conclusions from this study are hence based on small vibration amplitudes as different levels of excitation force is not examined.

8.1 Further work

As mentioned by the introduction, the work shown in this paper will be the basis for a successive study in indirect load estimation. The knowledge gained will feed the updating process of a finite element model needed for the dynamic analysis of wave action.

Acknowledgements

References

[1] R. Allemang. The modal assurance criterion (MAC): Twenty years of use and abuse. *Journal of Sound and Vibration*, Vol. 37(8):pp. 14–23, 2003.

[2] P. Avitabile. Modal space - back to basics. *Society of experimental mechanics Journal compilation*, December:pp. 1–2, 2007.

[3] N. Barltrop and A. Adams. *Dynamics of fixed marine structures*. Butterworth-Heinemann, UK, 3 edition, 1991.

[4] B. Blevins. *Formulas for natural frequency and mode shape*. Krieger Publishing Company, Malabar, Florida, USA, 1984.

[5] R. Brincker. On the application of correlation function matrices in OMA. *Mechanical Systems and Signal Processing*, 87:pp. 17–22, 2017.

[6] R. Brincker and C. Ventura. *Introduction to Operational Modal Analysis*. John Wiley and Sons, Ltd, UK, 2015.

[7] S. Chakrabarti. *Offshore structure modeling, Advanced series on ocean engineering*, volume 9. World Scientific Publishing Co. Pte. Ltd., 1994.

[8] R. Han and H. Xu. A simpled and accurate added mass model for hydrodynamic fluid-structure inter-action analysis. *Journal of the Franklin Institute, Volume 333, Issue 6*, 1996.

[9] A. Harvey. *Time series models*. Phillip Allan Publisher Ltd, 1981.

[10] M. Imregun and D. Ewins. Complex modes - origins and limits. *Proceedings of the International Modal Analysis Conference, IMAC*, 1:pp. 496 – 506, 1995.

[11] G. C. James, T. G. Carne, and J. P. Lauffer. The natural excitation technique (NExT) for modal param-eter extraction. *The International Journal of Analytical and Experimental Modal Analysis*, 10(4):pp. 260–277, 1995.

[12] M. Maheri and R. Severn. Experimental added-mass in modal vibration of cylindrical structures. *Engineering Structures*, 14 (3):pp. 163 – 175, 1992.

[13] P. Olsen, M. Juul, and R. Brincker. Condensation of the correlation functions in modal testing. *Submitted to Mechanical Systems and Signal Processing*, 2017.

[14] M. Pastor, M. Binda, and T. Harcarik. Modal assurance criterion. *Procedia Engineering 48*, 2012.

[15] M. Rahman and D. Bhatta. Evaluation of added mass and damping coefficient of an oscillating circular cylinder. *Applied Mathematical Modelling*, 17 (2):pp. 70–79, 1993.

[16] U. Tygesen, K. Worden, T. Rogers, G. Manson, and E. Cross. State-of-the-art and future directions for predictive modelling of offshore structure dynamics using machine learning. *Proceedings of the International Modal Analysis Conference, IMAC*, 2018.

[17] H. Vold, J. Knudrat, G. Rocklin, and R. Russell. A multi-input modal estimation algorithm for mini-computers. *SAE International Congress and Exposition*, Technical Paper 820194, 1982.

[18] V. Vu, M. Thomas, A. Lakis, and L. Marcouiller. Effect of added mass on submerged vibrated plates. *25th Seminar on machinery vibration, Canadian Machinery Vibration Association*, 2007.